



# Synthesis and characterization of Ni–Si<sub>3</sub>N<sub>4</sub> nanocomposite coatings fabricated by pulse electrodeposition

SEYYED MOHAMMAD NOORI

School of Metallurgy and Materials Engineering, College of Engineering, University of Tehran,  
P.O. Box 11155-4563, Tehran, Iran  
Mohammad.noori@alumni.ut.ac.ir

MS received 23 February 2018; accepted 17 July 2018; published online 12 February 2019

**Abstract.** Pure Ni and Ni–silicon nitride (Si<sub>3</sub>N<sub>4</sub>) nanocomposite coatings have been successfully fabricated on copper substrates by a pulse electrodeposition method employing the Watts bath. The obtained coatings were characterized with X-ray diffractometry and scanning electron microscopy. Also, surface hardness and the corrosion behaviour of the coatings were analysed by potentiodynamic polarization and electrochemical impedance spectroscopy in a 3.5% NaCl solution. It was found that incorporation of Si<sub>3</sub>N<sub>4</sub> particulates has reduced the crystallite size and also changed the growth orientation of the crystallite from (111) to (220) and (200) crystal planes. The co-deposition of Si<sub>3</sub>N<sub>4</sub> in the Ni matrix led to better properties of these coatings. Accordingly, the hardness value of nanocomposite coatings was about 80–140 Hv higher than that of pure nickel due to dispersion-strengthening and matrix grain refining and increased with the enhancement of incorporating Si<sub>3</sub>N<sub>4</sub> particle content. The presence of the Si<sub>3</sub>N<sub>4</sub> particulates slightly decreases the current efficiency. The current efficiency was decreased by increasing current density from 1 to 4 A dm<sup>−2</sup>. Moreover, the corrosion resistance of nanocomposite coatings was significantly higher than the pure Ni deposit. Also, the Ni–Si<sub>3</sub>N<sub>4</sub> coating produced at a density of 4 A dm<sup>−2</sup> showed the lowest corrosion rate (0.05 mpy).

**Keywords.** Composite coating; pulse electrodeposition; co-deposition; hardness; corrosion.

## 1. Introduction

Conventional metal coatings can no longer satisfy existing needs with progressing current industries. Many efforts have been made to reclaim and improve the properties of these coatings. One way is the creation of a secondary phase in the form of dispersion non-metallic particles, termed as composite coatings [1–3]. These coatings have the properties of a metallic matrix such as thermal and electrical conductivity, ductility and simultaneously the properties of dispersed particles in a matrix such as thermal stability, chemical stability and high hardness [4,5]. Among the various methods used to produce composite coatings, the electrodeposition method is widely used in laboratory conditions due to its low cost and simplicity of the procedure [6].

Nickel composite coatings have been specially considered for good mechanical, thermal, electrical and corrosion properties [7–9]. Later, by replacing the pulse current (PC) mode instead of direct current, some problems such as hydrogen embrittlement and less incorporation of nanoparticles in metal matrix was greatly resolved. It has also been reported that the use of PC and even pulse reverse current has led to a higher co-deposition of nanoparticles in the nickel matrix and hence higher corrosion resistance of these composite coatings [10–12]. Many parameters such as the electrolyte stirring rate [5], temperature and pH of the electrolyte, current density [13],

frequency [14], operating time, type and concentration of nanoparticles in electrolyte [15,16] are involved in deposition properties. Subsequently, change of each of these parameters can affect the thickness, coating structure, surface morphology and the amount of incorporating particles in deposit.

Silicon nitride (Si<sub>3</sub>N<sub>4</sub>) has very good properties such as low density, high strength, high failure toughening, good thermal shock, chemical resistance and excellent strength up to 1200°C. Hence, these nanoparticles are used in many cases in different matrices [17]. The ultimate properties of composite coatings are dependent on the amount of particle incorporation on deposit. Based on previous research, Ni–Si<sub>3</sub>N<sub>4</sub> composite coatings prepared at a concentration of 3 g l<sup>−1</sup> with about 9 vol% nanoparticles in deposit, exhibited good corrosion resistance [18]. It was also reported in a similar study that the highest co-deposition of Si<sub>3</sub>N<sub>4</sub> nanoparticles is an optimal state. In this manner, the maximum co-deposition is obtained at a concentration of 10–12 g l<sup>−1</sup> of nanoparticles. At higher concentration of Si<sub>3</sub>N<sub>4</sub>, the co-deposition decreased due to agglomeration of particle in the electrolyte [19]. However, this is different in the case of different particles and even in different matrices; for example, the greatest amount of zirconia in a nickel matrix is obtained in a bath containing 90 g l<sup>−1</sup> of this powder, which has the highest hardness and corrosion resistance [20,21]. Also, Si<sub>3</sub>N<sub>4</sub> powder showed the highest incorporation in a copper matrix at the concentration

of 40–35 g l<sup>-1</sup> [5,21]. Unlike previous cases, for TiO<sub>2</sub> particles in copper matrix, there is an incremental trend and at a concentration of 100 g l<sup>-1</sup>, the co-deposition of these particles reached about 9.5% [22]. The main purpose of this study is to investigate and compare Ni nanocomposite coatings with pure nickel deposits and also study the effect of current density on microstructure, microhardness and electrochemical behaviour of these coatings.

## 2. Experimental

The samples used in this study were copper sheets (purity >99%) with dimensions of 20 × 10 × 1 mm<sup>3</sup>, which were used as cathodes. The presence of oil, oxide and any kind of contamination on the surface of the sample can cause impairment in the electrodeposition process. Therefore, sample preparation is very important. The copper cathode was polished (by silicon carbide paper from 400 to 2000), degreased in acetone (for 1 min), dipped in HCl (15%) and finally washed in distilled water.

The pulse power supply and also Watts bath (in 300 cm<sup>3</sup>) were used for electrodeposition of samples. The electrolyte composition is presented in table 1. In this study, a high purity Si<sub>3</sub>N<sub>4</sub> powder of average size about 15 nm (which was provided from Penta Chemicals) was used without any treatment (figure 1). In order to control the agglomeration of Si<sub>3</sub>N<sub>4</sub> nanoparticles, the following procedure was performed: at first, this powder was added to water and then stirred for 24 h using a magnetic stirrer. After the bath reached a uniform temperature of 50°C, Si<sub>3</sub>N<sub>4</sub> powder was added to the bath at a concentration of 10 g l<sup>-1</sup> and was stirred in the bath for 1 h, so that all Si<sub>3</sub>N<sub>4</sub> particles were sufficiently moistened and uniformly suspended in the electrolyte. Also, before electrodeposition, the electrolyte was ultrasonicated for 0.5 h. During the deposition, a magnetic stirrer was used to create turbulence to prevent particles settling and suspend them. The distance between the cathode and the anode for each test was 5 cm and the stirring rate was also maintained at 200 rpm. Treatment time for all tests was 15 min. The deposition conditions in this study are summarized in table 2. The parameter studied in this study was current density, so that the nanocomposite deposition was performed at two current densities of 1 and 4 A dm<sup>-2</sup>.

**Table 1.** Chemical bath composition of pure and nanocomposite nickel coatings.

Composition	Concentration (g l <sup>-1</sup> )
NiSO <sub>4</sub>	300
NiCl <sub>2</sub>	40
H <sub>3</sub> BO <sub>3</sub>	30
SDS <sup>a</sup>	0.3
Si <sub>3</sub> N <sub>4</sub>	10

<sup>a</sup>Sodium dodecyl sulphate.

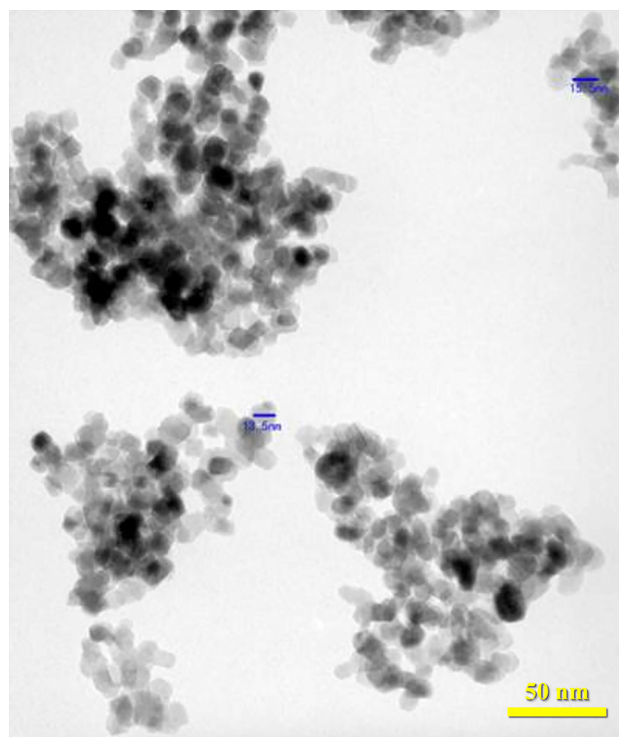


**Figure 1.** TEM image of Si<sub>3</sub>N<sub>4</sub> nanoparticles.

**Table 2.** General conditions for electrodeposition.

Parameter	Type or value
Electrolyte volume	300 cm <sup>3</sup>
Anode	Commercial Ni
Cathode	Copper sheet
pH	4.5
Temperature	50°C
Stirring rate	200 rpm
Treatment time	15 min
Frequency	10 Hz
Duty cycle	50%
Current type	Pulse
Current density	1 and 4 A dm <sup>-2</sup>

Surface morphology of the coating and uniformity of particles was investigated by using a scanning electron microscope (SEM) equipped EDS device. X-ray diffraction (XRD: Philips X'Pert Pro) analysis was performed on samples with Cu K $\alpha$  radiation ( $\lambda = 1.5406 \text{ \AA}$ ). The microhardness of coatings was measured five times with a load of 10 g and the mean value with the error bar was reported. Electrochemical experiments were carried out in 3.5% sodium chloride solution and in a conventional three electrode cell. Samples were used as a work electrode, a saturated calomel electrode as the reference electrode, and a platinum counter electrode. Potentiodynamic polarization tests were conducted

by using a Potentiostatic device (PGSTAT30) with a scan rate of  $1 \text{ mV s}^{-1}$ . The electrochemical impedance spectroscopy (EIS) was performed at a frequency range of 100 kHz–100 mHz with a range of  $\pm 10 \text{ mA}$ . The obtained data were analysed by selecting appropriate equivalent circuit and using Zview2 software.

### 3. Results and discussion

#### 3.1 Phase composition

Figure 2 shows the XRD pattern of pure Ni and Ni–Si<sub>3</sub>N<sub>4</sub> nanocomposite coatings. As seen in all cases, only the Ni peaks were identified. Since the volume fraction of Si<sub>3</sub>N<sub>4</sub> in the coating was less than 5%, the peak associated with this phase was not identified (this is referred from energy dispersive X-ray analysis (EDAX)). The crystallite size of pure Ni deposit and the Ni–Si<sub>3</sub>N<sub>4</sub> nanocomposite coating were determined using the Scherrer equation [23] and presented in table 3:

$$D = \frac{0.89\lambda}{\beta \cos \theta} \quad (1)$$

where  $\lambda$  is the wavelength for the X-rays,  $\beta$  is the full-width at half-maximum (FWHM) of the major diffraction peak and  $\theta$  is the diffraction angle of the XRD spectra. The crystallite sizes of pure Ni deposit and Ni–Si<sub>3</sub>N<sub>4</sub> nanocomposites

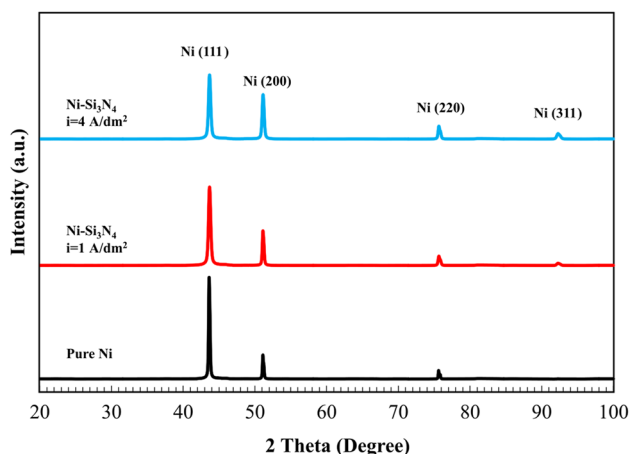


**Figure 2.** XRD pattern of pure nickel and Ni–Si<sub>3</sub>N<sub>4</sub> nanocomposite coatings.

**Table 3.** XRD parameters calculated from major peaks for pure nickel and Ni–Si<sub>3</sub>N<sub>4</sub> nanocomposite coatings.

	$2\theta$ (°)	FWHM (°)	Crystallite size (nm)
Pure Ni	43.65	0.108	98
$i = 1 \text{ A dm}^{-2}$	43.61	0.194	55
$i = 4 \text{ A dm}^{-2}$	43.64	0.321	33

were calculated and found to be about 98, 55 and 33 nm, respectively. It can be said that the addition of Si<sub>3</sub>N<sub>4</sub> nanoparticles has reduced the crystallite size. Moreover, addition of Si<sub>3</sub>N<sub>4</sub> nanoparticles has changed the growth orientation of the crystallite from (111) to (220) and (200) planes. The crystallization of Ni on (111) in pure nickel deposit was due to high atom density ( $1/2R^2\sqrt{3}$ ,  $R$  is the Ni atoms radius) and consequently lower surface energy. In composite coatings, some of the Ni<sup>2+</sup> ions were not capable of crystallization in the (111) plane, consequently they rest on the (200) and (220) planes. These results are in agreement with observations made by Chen *et al* [24].

#### 3.2 Surface morphology of coating

SEM images of the pure nickel and also Ni–Si<sub>3</sub>N<sub>4</sub> nanocomposite coatings which are presented in two magnifications of 200× and 2500×, are shown in figure 3. The addition of Si<sub>3</sub>N<sub>4</sub> nanoparticles increased the smoothness of the nanocomposite coating. The reason for this is the absorption of nanoparticles on the surface, which accelerates the nucleation rate and delays the growth of the coating, which ultimately leads to the formation of smaller crystals in the coating. Also, when the amount of nanoparticles in the electrolyte is in excess, it leads to their agglomeration at the surface of the coating. It can be seen that pure nickel deposit possessed a truncated pyramidal structure, which is a common morphology for pure Ni electrodeposit [25,26]. The addition of Si<sub>3</sub>N<sub>4</sub> nanoparticles changes the structure and morphology of coatings. So, for Ni–Si<sub>3</sub>N<sub>4</sub> nanocomposite coatings, the morphology of the crystals is relatively irregular polygonal.

Changing the current between zero and positive values in a pulse mode leads to charging and discharging a double-layer capacitor around the cathode allowing better absorption of the particle into the coating. In pulse electrodeposition, current density and changes between on-time and off-time play an important role in the deposition of nanoparticles. High-current densities for a short time result in entry of the maximum number of particles into the coating. During on-time of current, Si<sub>3</sub>N<sub>4</sub> particles which were surrounded by Ni<sup>2+</sup> ions move towards the cathode, but the nickel ions flux is much larger than that of Si<sub>3</sub>N<sub>4</sub> particles. Furthermore, at current off-time, only Si<sub>3</sub>N<sub>4</sub> particles are transferred to the cathode due to turbulence and absorbed by the surface.

Based on EDAX results shown in table 4, it is observed that on increasing current density, the co-deposition of Si<sub>3</sub>N<sub>4</sub> nanoparticles increases in the nickel matrix. Moreover, by increasing the current density from 1 to 4 A dm<sup>−2</sup>, the weight fraction of Si<sub>3</sub>N<sub>4</sub> deposited in the coating increased from ~7 to ~9%. As the current density increases, the tendency to absorb nanoparticles towards the cathode surface increases, which is based on Guglielmi's model [27]. In fact, the adsorption rate of nanoparticle is controlling the process. It has also been reported that in current density higher than 8 A dm<sup>−2</sup> due to increased hydrogen evolution, deposition efficiency decreases and result in lower co-deposition of Si<sub>3</sub>N<sub>4</sub> particles



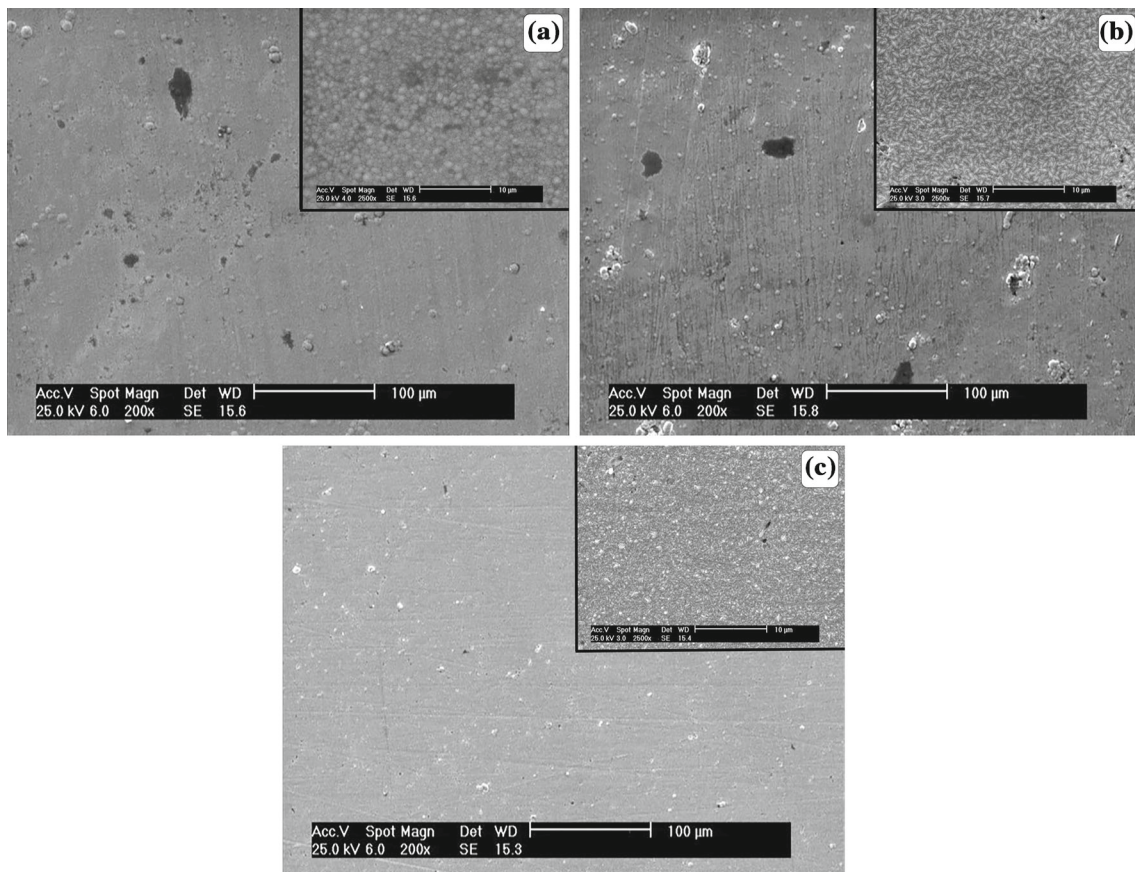


**Figure 3.** Surface morphology of (a) pure Ni coating, (b) Ni-Si<sub>3</sub>N<sub>4</sub> nanocomposite coating prepared at 1 A dm<sup>-2</sup> and (c) Ni-Si<sub>3</sub>N<sub>4</sub> nanocomposite coating prepared at 4 A dm<sup>-2</sup>.

**Table 4.** EDAX results of pure nickel and Ni-Si<sub>3</sub>N<sub>4</sub> nanocomposite coatings.

	Ni	Si	N
Pure Ni	100	0	0
$i = 1 \text{ A dm}^{-2}$	93.23	2.72	4.25
$i = 4 \text{ A dm}^{-2}$	91.11	3.45	5.44

in the coating. The formation of Ni(OH)<sub>2</sub> on the cathode surface will contribute to the precipitation process which is in agreement with Shi *et al* results [22]. Up to  $\sim 8 \text{ A dm}^{-2}$  current densities, the reducing trend of nanoparticles co-deposition is that the deposition rate of the nickel region is faster, while the amount of particles is much lower in the coating. As seen, the smoothness of coating prepared at  $4 \text{ A dm}^{-2}$  was higher than the other samples.

Figure 4 illustrates the effects of current density on current efficiency. The current efficiency ( $\eta$ ) of this process can be calculated using the following equation:

$$\eta(\%) = \frac{m}{MI_a t / zF} \quad (2)$$

where  $z$  is valence,  $m$  is mass of deposit,  $M$  is molar mass of nickel ( $58.7 \text{ g mol}^{-1}$ ),  $I_a$  is average current and  $t$  is the treatment time.  $I_a$  is average current and is defined as:

$$I_a = I_p \gamma = \frac{I_p T_{on}}{T_{on} + T_{off}} \quad (3)$$

where  $I_p$  is the peak current and  $\gamma$  is the duty cycle. It was observed that on increasing the current density the  $\eta$  value decreased. Two reasons for this behaviour was mentioned: (i) at high-current densities, the consumption rate of Ni<sup>2+</sup> ions increases and leads to a decrease in the concentration of these ions at the cathode surface and ultimately decreases the current efficiency and (ii) moreover, the decomposition of water and hydrogen evolution caused the increase in current loss.

### 3.3 Microhardness

The microhardness measurements which were performed for pure nickel and also Ni-Si<sub>3</sub>N<sub>4</sub> nanocomposite coatings are shown in figure 5. Nanocomposite coatings have a higher microhardness value compared to the pure nickel coating ( $220 \pm 7 \text{ Hv}$ ). As discussed before, Si<sub>3</sub>N<sub>4</sub> nanoparticles

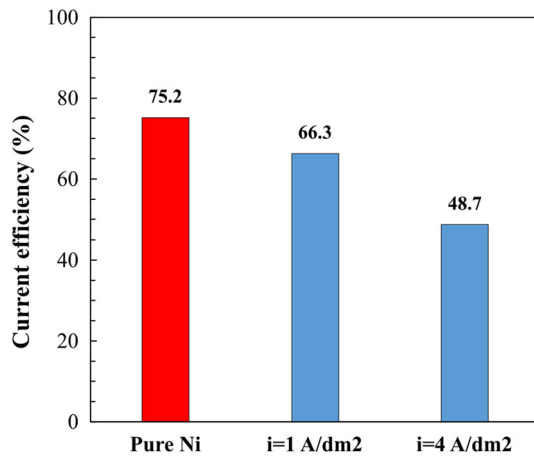


**Figure 4.** Effect of current density on current efficiency of electrodeposited coatings.

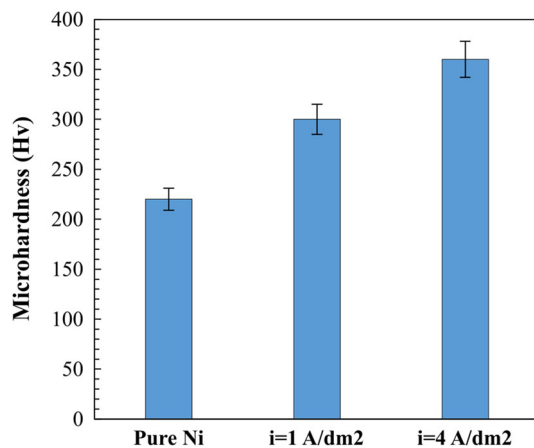


**Figure 5.** Microhardness of pure Ni and Ni–Si<sub>3</sub>N<sub>4</sub> nanocomposite coatings.

prevent the growth of nickel crystals and change the plastic deformation of nickel matrix, so the crystallite size was reduced. The embedding of Si<sub>3</sub>N<sub>4</sub> nanoparticles acts as a dispersive strengthening mechanism along with grain refinement leading to higher hardness value of composite coatings. Moreover, these effects became more tangible by increasing the amount of particles in composite coatings, and thus higher value of hardness will be obtained. The interaction between tensile fields around the coatings and dislocations, as well as the physical collisions, can lead to particle cutting or the formation of Orowan rings. Good distribution of nanoparticles at low distances will increase the effectiveness of the Orowan mechanism and consequently result in higher hardness of coating. Moreover, on increasing the current density, co-deposition of Si<sub>3</sub>N<sub>4</sub> nanoparticles increased. Therefore, the nanocomposite coating produced at a density of 4 A dm<sup>-2</sup> exhibits a higher hardness (360 ± 11 Hv) relative to 1 A dm<sup>-2</sup> (300 ± 9 Hv).

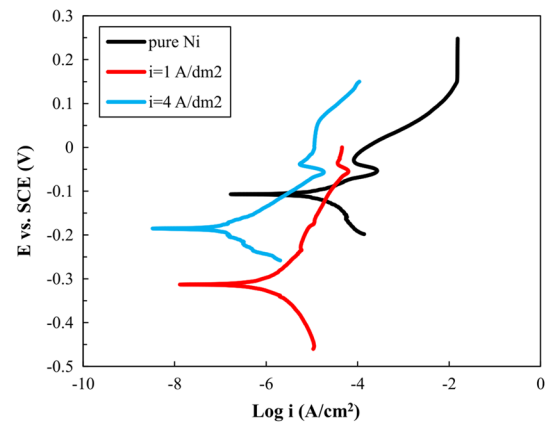


**Figure 6.** Potentiodynamics polarization curves for pure nickel and Ni–Si<sub>3</sub>N<sub>4</sub> nanocomposite coatings.

### 3.4 Corrosion studies

**3.4a Potentiodynamic polarization:** Figure 6 shows the Tafel polarization curves for pure nickel and Ni–Si<sub>3</sub>N<sub>4</sub> nanocomposite coatings in a 3.5% sodium chloride solution. The values of corrosion potential ( $E_{\text{corr}}$ ), corrosion current density ( $i_{\text{corr}}$ ), anodic/cathodic Tafel slopes ( $\beta_a/\beta_c$ ) and corrosion rate (CR) derived from polarization curves are summarized in table 5. The CR was calculated from the following equation:

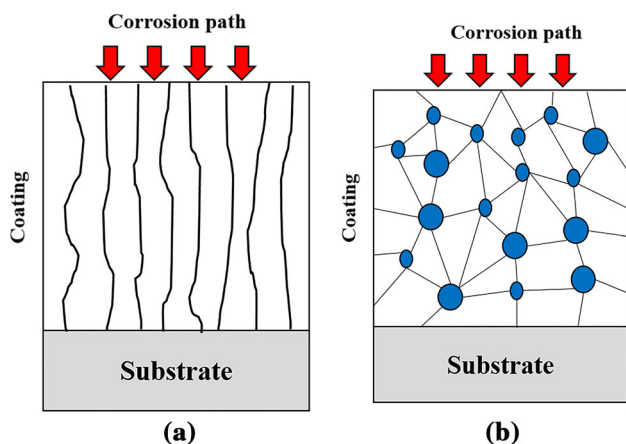
$$\text{CR (mpy)} = i_{\text{corr}} (\text{A cm}^{-2}) \times \frac{1}{zF(\text{As})} \times \frac{M_{\text{Ni}}(\text{g mol}^{-1})}{\rho_{\text{Ni}}(\text{g cm}^{-3})} \times \frac{1 (\text{in})}{2.54 (\text{cm})} \times \frac{365 \times 24 \times 3600 (\text{s})}{1 (\text{year})} \times 10^3 \quad (4)$$

The nanocomposite coatings exhibit a lower corrosion potential and lower corrosion current density compared to pure nickel deposit. The reason for the higher corrosion resistance of nanocomposite coatings compared to pure nickel can be found in the following three cases:

- (1) Ceramic particles such as Si<sub>3</sub>N<sub>4</sub> have a high corrosion resistance. So long as these particles are dispersed on nanocomposite coating, the coating surface in contact with the corrosive environment is reduced.
- (2) The dispersed Si<sub>3</sub>N<sub>4</sub> particles in a nickel matrix act as a barrier to corrosion, causing a change or even development of the corrosion path and reduces the CR.
- (3) The existence of Si<sub>3</sub>N<sub>4</sub> nanoparticles in the nickel matrix leads to a change in the grain structure of coating from columnar to axial (figure 7). In the columnar structure for pure nickel deposit, there are direct paths that the corrosive solution can easily develop along and move at high rate. But in nanocomposite coatings that have an equiaxed structure, short paths and twists in the sheet are

**Table 5.** Parameters obtained from the polarization curves for pure nickel and Ni-Si<sub>3</sub>N<sub>4</sub> nanocomposite coatings.

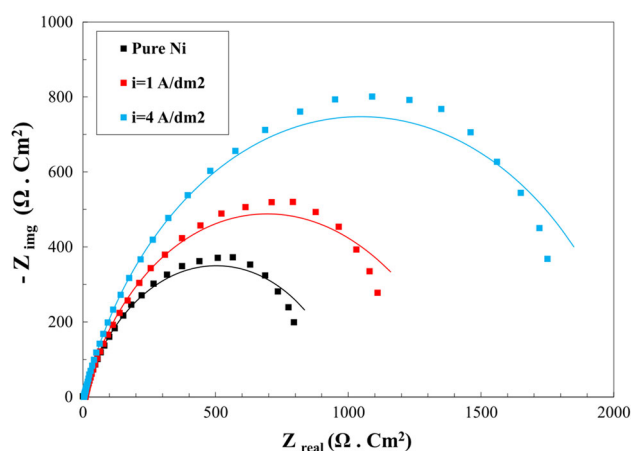
Sample	$\beta_a$ (V dec <sup>-1</sup> )	$\beta_c$ (V dec <sup>-1</sup> )	$E_{\text{corr}}$ (V)	$i_{\text{corr}}$ (A cm <sup>-2</sup> )	CR (mpy)
Pure Ni	0.0792	0.0453	-0.103	$1.41 \times 10^{-5}$	5.95
$i = 1 \text{ A dm}^{-2}$	0.1382	0.1512	-0.304	$1.67 \times 10^{-6}$	0.70
$i = 4 \text{ A dm}^{-2}$	0.0613	0.0587	-0.193	$1.14 \times 10^{-7}$	0.05

**Figure 7.** Schematic microstructure and corrosion path towards surface substrate for (a) pure nickel and (b) Ni-Si<sub>3</sub>N<sub>4</sub> nanocomposite coatings.

replaced by a straight and long path, which reduces the CR [28].

Differences in the anode and cathode Tafel values for pure nickel and nanocomposite coatings are consistent with the changes caused by surface correction by co-deposition of nanoparticles. In fact, the presence of Si<sub>3</sub>N<sub>4</sub> nanoparticles affects the kinetic of anodic and cathodic reactions. Corrosion potential ( $E_{\text{corr}}$ ) of nanocomposite coatings is also less pronounced, indicating the nature of the cathodic protection of these coatings, which was previously investigated by Ramalingam *et al* [15]. Negative displacement of plots towards lower values is related to the reduction of the special active surface of the cathode, which results from the absorption of Si<sub>3</sub>N<sub>4</sub> nanoparticles on the surface and may be related to the reduction of anionic transfer of these particles. Generally, nanocomposite coatings have a lower chemical activity compared to pure nickel, resulting in better chemical stability in an external environment. It is also observed that by increasing the current density from 1 to 4 A dm<sup>-2</sup>, the CR decreased from 0.70 to 0.05 mpy. This can be explained by the fact that more Si<sub>3</sub>N<sub>4</sub> particles are deposited in the coating, which was investigated in the previous sections.

**3.4b Electrochemical impedance spectroscopy (EIS):** In order to investigate more accurately the corrosion behaviour of the applied coatings, EIS test was used. Figure 8 shows

**Figure 8.** Nyquist plots obtained for pure Ni and Ni-Si<sub>3</sub>N<sub>4</sub> nanocomposite coatings.

the Nyquist plots obtained from the EIS test in 3.5% sodium chloride solution. The identification of corrosion enhancement mechanism is necessary to provide an equivalent circuit. The corrosion resistance of the pure nickel coating was based on a passive layer. Based on previous research, the boundary between the nickel clusters is corroded and dipped, so this is a good place for failure of the passive layer [29]. However, in Ni-Si<sub>3</sub>N<sub>4</sub> nanocomposite coatings, the boundary between the Si<sub>3</sub>N<sub>4</sub> particles and the nickel matrix is a suitable place to breakdown the passive layer. Since the localized corrosion occurs in both cases, Randles circuit can't be used in this system. Here, there are two different layer areas (passive and corroded), and for each one a double layer should be considered. These double layers are shown by capacitors ( $C_{\text{coat}}$  for the passive area and  $C_{\text{dl}}$  for corroded area). The actual surfaces are not smooth, uniform, and not ideal, so a constant phase element (CPE) was used instead of the ideal capacitor, which is expressed in terms of the following equation:

$$Z_{\text{CPE}} = \frac{1}{[C(j\omega)^n]} \quad (5)$$

where  $Z_{\text{CPE}}$  is impedance,  $j$  is the second root of 1,  $\omega$  is the frequency,  $C$  is the capacitance and  $n$  is the non-ideal value of the capacitor, which is a number between 0 and 1. The final circuit used to fit to the experimental data and corresponding values is given in figure 9 and table 6, respectively.

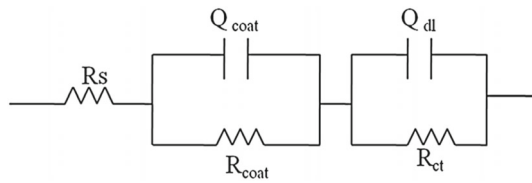


**Figure 9.** Equivalent circuit used for pure Ni and Ni-Si<sub>3</sub>N<sub>4</sub> nanocomposite coatings.

**Table 6.** Parameters obtained from Nyquist plots for pure Ni and Ni-Si<sub>3</sub>N<sub>4</sub> nanocomposite coatings.

Sample	$R_s$ ( $\Omega$ cm <sup>2</sup> )	$R_{coat}$ ( $\Omega$ cm <sup>2</sup> )	$C_{dl}$	$R_{ct}$ ( $\Omega$ cm <sup>2</sup> )
Pure Ni	5.2	59.1	0.193	989
$i = 1$ A dm <sup>-2</sup>	6.6	44.7	0.091	1384
$i = 4$ A dm <sup>-2</sup>	6.8	39.8	0.008	2064

It is observed that there is a great deal of consistency between the diagrams that show the accuracy of the selected circuit to model the corrosion conditions of these coatings. In this case, the Nyquist plots have only one semicircle and provide information about the polarity and the charge in the electrode/electrolyte interface. Also, the surface heterogeneity can be related to the value of CPE [30].

The charge transfer resistance ( $R_{ct}$ ) of the nanocomposite coatings is higher than the pure nickel coating (989  $\Omega$  cm<sup>2</sup>), indicating a higher corrosion resistance. It is also observed that by increasing the current density from 1 to 4 A dm<sup>-2</sup>, the corrosion resistance increased from 1384 to 2064  $\Omega$  cm<sup>2</sup>. This observation was due to higher amount of Si<sub>3</sub>N<sub>4</sub> in the coatings which was discussed previously. On increasing the amount of Si<sub>3</sub>N<sub>4</sub> in the coating, the charge transfer resistance ( $R_p$ ) increased and CPE decreased.

#### 4. Conclusion

The pure nickel and Ni-Si<sub>3</sub>N<sub>4</sub> nanocomposite coatings were successfully applied using a pulsed electrodeposition method. The following results were obtained:

- (1) The presence of Si<sub>3</sub>N<sub>4</sub> nanoparticles in the coating led to a reduction in the crystallite size, change in the orientation of the crystals, and also slightly decreased the current efficiency.
- (2) Hardness and corrosion resistance of nanocomposite coatings were higher than pure nickel, which was related to the presence of co-deposited nanoparticles in the coating.
- (3) Increasing current density from 1 to 4 A dm<sup>-2</sup> leads to an increase in the amount of co-deposition of particles in the coating.

- (4) Nanocomposite coating produced at a density of 4 A dm<sup>-2</sup> showed the highest hardness (360 Hv) and the lowest CR (0.05 mpy).

#### References

- [1] Hou K H, Sheu H H and Ger M D 2014 *Appl. Surf. Sci.* **308** 372
- [2] Aruna S T and Srinivas G 2015 *Surf. Eng.* **31** 708
- [3] Bajwa R S, Khan Z, Bakolas V and Braun W 2016 *Acta Metall. Sin.* **29** 8
- [4] Agarwala R C and Agarwala V 2003 *Sadhana* **28** 475
- [5] Eslami M, Saghaian H and Golestani-fard F 2014 *Appl. Surf. Sci.* **300** 129
- [6] Bakht B, Akbari A, Nasirpour F and Hosseini M G 2014 *Appl. Surf. Sci.* **307** 351
- [7] Gheorghies C, Carac G and Stasi I V 2006 *J. Optoelectron. Adv. Mater.* **8** 1234
- [8] Chen X H, Chen C S, Xiao H N, Cheng F Q, Zhang G and Yi G J 2005 *Surf. Coat. Technol.* **191** 351
- [9] Kang J X, Zhao W Z and Zhang G F 2009 *Surf. Coat. Technol.* **203** 1815
- [10] Reddy R M, Praveen B M, Chandrappa K G and Nayana K O 2016 *Surf. Eng.* **32** 501
- [11] Lajevardi S A and Shahrabi T 2010 *Appl. Surf. Sci.* **256** 6775
- [12] Zoikis-Karathanasis A, Pavlatou E A and Spyrellis N 2010 *J. Alloy Compd.* **494** 396
- [13] Asnavandi M, Ghorbani M and Kahram M 2013 *Surf. Coat. Technol.* **216** 207
- [14] Lekka M, Zendron G, Zanella C, Lanzutti A, Fedrizzi L and Bonora P L 2011 *Surf. Coat. Technol.* **205** 3438
- [15] Ramalingam S, Muralidharan V S and Subramania A 2009 *J. Solid State Electrochem.* **13** 1777
- [16] Srivastava M, Grips V W and Rajam K S 2008 *Mater. Lett.* **62** 3487
- [17] Li Q, Yang X, Zhang L, Wang J and Chen B 2009 *J. Alloy Compd.* **482** 339
- [18] Reddy R M, Praveen B M, Kumar C P and Venkatesha T V 2017 *Surf. Eng. Appl. Electrochem.* **53** 258
- [19] Kasturibai S and Kalaignan G P 2014 *Bull. Mater. Sci.* **37** 721
- [20] Arghavanian R and Parvini-Ahmadi N 2011 *J. Solid State Electrochem.* **15** 2199
- [21] Zhu J, Liu L, Hu G, Shen B, Hu W and Ding W 2004 *Mater. Lett.* **58** 1634
- [22] Shi L, Sun C, Gao P, Zhou F and Liu W 2006 *Appl. Surf. Sci.* **252** 3591
- [23] Shewmon P ed. 2016 *Diffusion in solids* (Berlin: Springer)
- [24] Chen L, Wang L, Zeng Z and Xu T 2006 *Surf. Coat. Technol.* **201** 599
- [25] Pathak S et al 2011 *Surf. Coat. Technol.* **205** 3651
- [26] Godon A et al 2011 *Mater. Charact.* **62** 164
- [27] Guglielmi N 1972 *J. Electrochem. Soc.* **119** 1009
- [28] Gül H, Kılıç F, Uysal M, Aslan S, Alp A and Akbulut H 2012 *Appl. Surf. Sci.* **258** 4260
- [29] Sajjadnejad M, Omidvar H, Javanbakht M and Mozafari A 2017 *J. Alloy Compd.* **704** 809
- [30] Solmaz R, Altunbaş E and Kardaş G 2011 *Mater. Chem. Phys.* **125** 796